NATURAL CONVECTION DRIVEN HEAT TRANSFER IN FLUIDS WITH STRONGLY VARIABLE PROPERTIES: A PARTICLE IMAGE VELOCIMETRY STUDY

V. Valori[1,2], G.E. Elsinga[2], M. Rohde[1]

[1]Faculty of Applied Sciences,
[2]Faculty of Mechanical Engeneeing,
Delft University of Technology, The Netherlands
V.Valori@tudelft.nl; G.E.Elsinga@tudelft.nl; M.Rohde@tudelft.nl

M.J. Tummers[2], J. Westerweel[2], T.H.J.J. van der Hagen[1]
[1]Faculty of Applied Sciences,
[2]Faculty of Mechanical Engeneeing,
Delft University of Technology, The Netherlands

ABSTRACT

The High Performance Light Water Reactor (HPLWR) is one of the six innovative nuclear energy systems proposed by the Generation IV International Forum. The use of water at supercritical pressure as the coolant in the HPLWR allows a significative increase of the thermal efficiency of the power plant, a reduction in size and complexity of the system and a safety improvement with respect to the use of two phase flows.
Fluids at supercritical pressure are characterized by a sharp change of properties, which may lead to an enhancement or deterioration of their heat transfer properties, whose underlying mechanisms are mainly driven by buoyancy and acceleration effects. The motivation of this research is therefore to understand the effect of the sharp change of properties in the fluid flow structure and turbulence production.

This work focuses on the influence of buoyancy in particular. The effect of the strongly varying properties, which are far beyond the so-called Boussinesq approximation, was experimentally studied in a water-filled, cubical Rayleigh-Bénard cell using Particle Image Velocimetry (PIV). A temperature difference of 40 K is imposed between the bottom and top plate of the cell, ensuring non-Boussinesq conditions. These experiments were conducted at Rayleigh and Prandtl numbers of 6.8×10^8 and 4.4, respectively. For the first time in literature, the instantaneous and averaged flow structures under non-Bousinesq conditions have been experimentally determined on a cross section of the whole domain. Results reveal a slight asymmetric behavior of the fluid due to the large temperature difference between the bottom and the top plates of the cell, which is a sign of non-Boussinesq effects. The data provided in this study can be used to gain a more in depth understanding of the effect of the strongly varying properties of supercritical fluids on natural convection phenomena in supercritical water cooled reactors.

KEYWORDS

Rayleigh-Bénard convection, Non-Boussinesq conditions, Particle Image Velocimetry, supercritical fluids.

1 INTRODUCTION

Fluids at supercritical pressure are characterized by a sharp change of properties as function of temperature and a peak of the specific heat capacity close to the critical point. Their properties change from a liquid-like to a gas-like state in a continuous way. At the same time, their specific heat capacity has a sharp peak, defining the so-called pseudocritical temperature. In Figure 1 a plot of some properties of water around its critical point is shown.

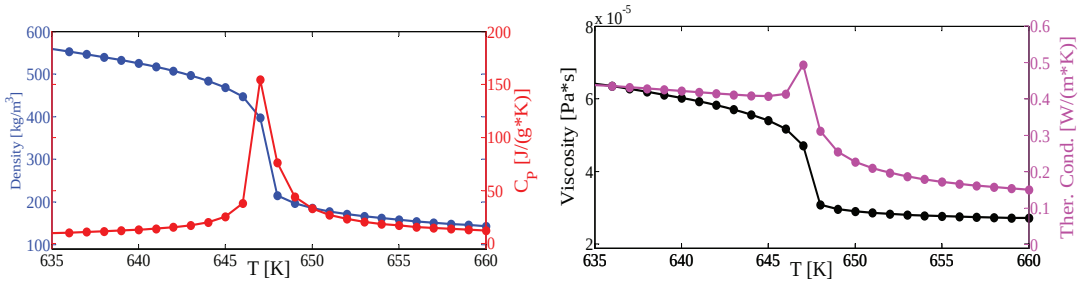

Figure 1: Fluid properties of water at 22.08 MPa. Left) density and specific heat at constant pressure versus temperature. Right) viscosity and thermal conductivity versus temperature. [Properties taken from REFPROP version 7]. Notice the large property gradient near the critical point (647.096 K, 22.064MPa, water).

Because of their properties supercritical fluids are attractive as cooling fluids for power plants. Their use allows the thermal efficiency of the power plant to increase from 33-35% of modern Nuclear Power Plants (NPPs) to 45-50% of supercritical cooled power plants [1]. Moreover, supercritical cooled NPPs are characterized by a compact design of the reactor, which corresponds to a reduction in size and complexity of the power plant.

Because of the continuous change of properties from the liquid-like to the gas-like phase of fluids at supercritical pressure, phenomena like dryout crisis, which characterize boiling water reactors (BWR), are not present in supercritical cooled power plants. This aspect can be seen as a safety improvement of SCWRs with respect to BWRs. Supercritical fluids, however, may show both heat transfer enhancement as well as heat transfer deterioration. The background of these different heat transfer regimes has not been understood yet and their heat trnsfer behaviour is therefore unpredictable.

The relevance of the changes in the heat transfer behavior and its relation with the fluid mechanics of fluids at supercritical pressure has been recently reviewed in J. Y. Yoo, (2013) [3]. Conditions of heat transfer deterioration are characterized by a sharp peack of the wall temperature of the cooled pipe. At such conditions the average velocity profiles and shear stresses are modified dramaticaly. In particuar it has been observed [Kurganov and Kaptil'ny (1992)] [2] a tipical M-shaped velocity profile in correspondece to a peack of the pipe wall temperature.
In a pipe flow mainly two effects have been identified as significant contributors to the quality of the heat transfer: the effect of buoyancy and the one of acceleration due to thermal expansion. In particular, it has been shown [Fewster and Jackson, 2004[4]] that the effect of buoyancy plays a positive role in case of downward pipe flows and a negative role in upward flows. This is particularly important for mixed convection, which can be found in nuclear reactor cores.

The present paper focuses on the effects of buoyancy on a natural convection system with the aim of understanding the influence of the effect of variable properties on the fluid flow and turbulence. A Rayleigh-Bénard system (RB) has been studied at conditions which goes far beyond the Boussinesq approximation. In the Boussinesq approximation, the fluid density is assumed to be constant except in the buoyancy term of the Navier-Stokes equations and all the other fluid properties are assumed constant. In the present paper a case has been studied in which the

volumetric thermal expansion coefficient and the kinematic viscosity change significantly with temperature, therefore, this dependence cannot be neglected. There are several earlier studies in literature which focus on Rayleigh-Bénard convection at non-Boussinesq (NB) conditions. In Ahlers *et al.* 2006 [5] an experimental and theoretical study on the effects of NB conditions on the Nusselt and Reynolds number is presented. They fluid chosen in their study is water at atmospheric pressure, which shows significant changes of the kinematic viscosity and the volumetric thermal expansion coefficient, in the range of the temperature considered. In similar conditions, a DNS study has been perfored with the purpose of analyzing the flow organization of Rayleigh-Bénard convection with variable properties [Sugiyama et al. 2009 [6]]. To complement the DNS study of Sugiyama on the flow organization of a RB system under NB conditions, experimental evidence is required, preferably of the entire flow domain.
Particle Image Velocimetry (PIV) has been applied to measure the entire instantaneous flow field on a vertical cross section of the domain. PIV has been used by [Xia et al. 2003 [7]] in a RB cell, but at Boussinesq conditions. In the present study, PIV will be applied at NB conditions with the aim of further investigating the effects of variable properties in water at atmospheric pressure. The characteristics of the average velocities and the RMSs of the velocities on a vertical cross section of the domain, obtained from PIV measurements, are studied in details. Small differences between Boussinesq and NB conditions have been observed. The results are also compared to the existing Grossman-Lohse theory, reviewed in Ahlers et al., 2009 [8], which describes the Reynolds and Nusselt dependencies on the Rayleigh and Prandtl numbers. Good agreement has been found between the experiments and this G.-L. theory, which was able to predict also the Reynolds number at the NB conditions experimentally studied.

2 EXPERIMENTAL SET-UP

The experimental set-up used to study the effects of variable properties on natural convection, mainly consists of two parts: a Rayleigh-Bénard cell and the equipment for Particle Image Velocimetry (PIV) measurements. Planar PIV measurements have been done in a vertical section of a cubic convection cell, at half depth of the domain. In Figure 2 a picture of the set-up, indicating its main components, is reported.

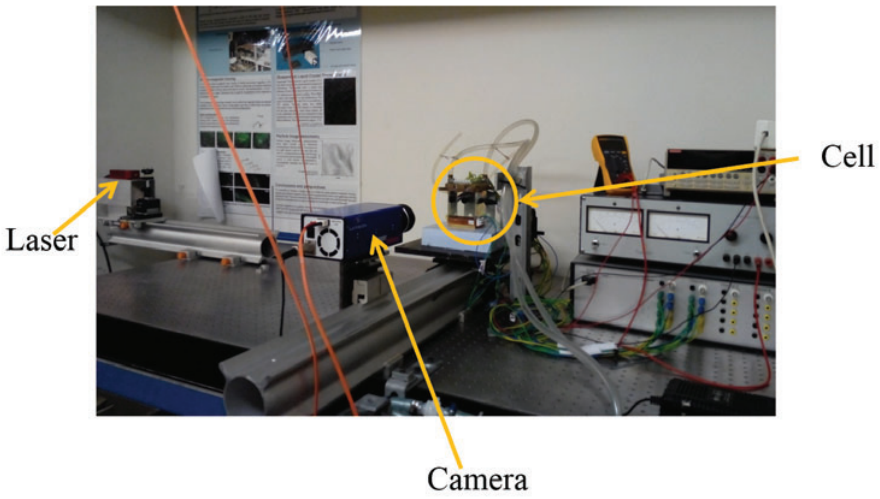

Figure 2: Picture of the set-up with indications of the RB convection cell and the instrumentation for PIV measurement.

2.1 Rayleigh-Bénard cell

The Rayleigh-Bénard cell used for the experiments is a cube of 77 mm inner length (H). It is made of glass vertical walls and two horizontal copper plates. The four vertical glass walls are 1.2 mm thick. The glass allows us to see through the walls of the cell, in order to perform optical measurements. The cell is silicon sealed and it has been designed to work with fuids at atmospheric pressure.
The bottom copper wall is electrically heated. The heating is realized by using an electrical heating strip, glued below the bottom copper plate. The electrical power given to the strip can be regulated to warm up the bottom plate to the desired temperature. The top copper wall is water cooled. The flow rate of the water through the upper plate is regulated in order to allow a maximum of 0,1°C of temperature difference between the water entering and exiting the plate. The temperature of the water can be regulated to cool down the top plate to the desired temperature. Four thermistors are located in each one of the horizontal walls to monitor the uniformity of the temperature in the plates. The thermistors are made of epoxy coated NTC of type C100. A schematic drawing convection cell is shown in Figure 3. The cell is slightly tilted, less than 3 degrees on both the X and Y direction, in order to reduce the occurrence of flow reversals.

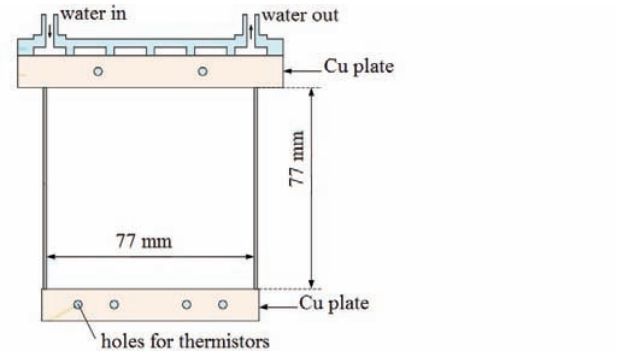

Figure 3: Scheme of a vertical section of the Rayleigh-Bénard cell [Figure taken and adapted from [10]]

2.2 PIV equipment

The equipment for the PIV measurements consists of one camera, a diode laser, which illuminates a vertical section of the domain and particles, that have been inserted into the fluid flow. An Imager Intense PIV camera from LaVision, with a resolution of 1088 X 1040 pixels has been used for the recordings. A Pegasus diode laser with a power of 400 mW and a wave length of 520 nm has been used for the illumination of the measurement section. Two kinds of particles have been used for the experiments with water and methanol. In water, fluorescent particles have been applied with the purpose of avoiding reflections of the laser light in the lateral glass walls of the cell and improving the quality of the measurements close to the wall. The fluorescent particles emit in a wave length that is different from the wave length of the laser and, for this reason, the laser light reflected by the glass lateral walls can be filtered out by a filter placed in front of the camera. The fluorescent particles are Fluostar particles with a diameter of 13 μm and density of 1,1 g/cm^3. The fluorescent dye is Rhodamine B, which is excited by a wave length of 550 nm and emits at 580 nm. For the experiments with methanol it was not possible to use fluorescent particles for reasons of chemical compatibility of the particles with alcohols (these particles dissolve in methanol). Silver coated particles produced by Dantec have been used in methanol instead. These particles have a diameter of 10 μm and density of 1,4 g/cm^3. In the experiments done with this kind of particles a background subtraction has been applied to the camera recordings, with the aim of reducing the effect of reflections of the laser light in the glass walls in the images. The image of the background which has been subtracted to the camera records consists of an average of more than 100 images. The averaging process deletes the particles, which are in different positions in each one of the several recordings and leaves the constant parts of the image, like the walls with light reflections. The subtraction of the time average image of the background allows us to subtract the effect of the reflection onto the vertical glass walls.

3 RESULTS

The results of PIV experiments in a Rayleigh-Bénard cell are shown, focusing on the time averages and the RMSs of the velocities within a vertical plane at half width of the cell. Two different experimental conditions have been studied, which have been called the non-Boussinesq (NB) and the Boussinesq case. At NB conditions the temperature difference between the bottom and the top plate of the cell leads to property differences, which are beyond the Boussinesq approximation, while at Boussinesq conditions the temperature difference applied to the two horizontal plates of the cell results in small changes of properties, which are more within the Boussinesq approximation. The two experiments have been done in the same set-up, working at almost the same Rayleigh and Prandtl number, as shown in Table 1. The Rayleigh and Prandtl numbers are the two non-dimensional parameters which govern the flow, obtained after non-dimensionalization of the Navier-Stokes equations.
The Rayleigh number represents the ratio between the thermal driving buoyancy force and the viscous force, defined as:

$$\mathbf{Ra} \equiv \frac{\alpha \cdot g \cdot \nabla T \cdot H^3}{\nu \cdot \kappa} \tag{1}$$

where α is the volumetric thermal expansion coefficient of the fluid, g is the gravitational acceleration (9.81 m/s^2), ∇T is the difference of temperature between the hot bottom plate and the cold top plate of the cell, ν is the kinematic viscosity of the fluid and κ is the thermal diffusivity of the fluid. All the properties in the non-dimensional numbers are taken at the average temperature between the bottom and top wall temperatures of the cell, indicated as T_m.
The Prandtl number is defined as the ratio between the diffusion of momentum and the diffusion of heat:

$$\mathbf{Pr} \equiv \frac{\nu}{\kappa} \tag{2}$$

In order to keep the same Rayleigh number in the same set-up, both for Boussinesq and non Boussinesq case, the experiment at Boussinesq conditions has been done with methanol.
Other two non-dimensional numbers important to the experiments are the Reynolds, **Re** and the Nusselt, **Nu** number. The Reynolds number is defined as:

$$\mathbf{Re} \equiv \frac{U \cdot H}{\nu} \tag{3}$$

where U is the velocity of the large scale circulation of the flow, which represents also the integral velocity scale of the flow; H is the integral length scale of the flow, which is the dimension of the cubical cell and ν is the kinematic viscosity of the fluid. The Nusselt number is defined as:

$$\mathbf{Nu} \equiv \frac{Q \cdot H}{\lambda \cdot \nabla T} \tag{4}$$

where Q is the heat flux trough the cell, H is the distance between the top and the bottom plate, λ is the thermal conductivity of the fluid and ∇T is the temperature difference between the bottom and the top wall temperatures.
The values of the properties of both water and methanol have been taken from REFPROP version 9.1.
In table 1 the experimental conditions of the two cases are reported, together with an example of the changes of the values of two properties between bottom and top plate of the cell. The two properties considered are the volumetric thermal expansion coefficient (α) and the kinematic viscosity (ν). They are the properties which change the most in water at atmospheric pressure.
In table 2 conservative values of the relative uncertainties of the experimental and the calculated

quantities are reported. The calculted quantities are non-dimensional numbers, which have been calculated from the measured quantities and the fluid properties taken from REFPROP version 9.1. The uncertainties in the calculated quantities are due to the uncertainties in the measured quantities.

Table 1: Left) Experimental conditions and comparison between the relative changes of α and ν from the bottom to the top of the cell. All the properties in the non dimensional numbers are taken at the average temperature between the bottom and top wall temperatures of the cell (indicated as T_m). The values of the properties of both water and methanol have been taken from REFPROP version 9.1. Working pressure: atmospheric pressure, in both cases.

Table 2: Right) Relative uncertainties of the measured (H, ∇T, U, U_{RMS}) and calculated (**Ra**, **Pr**, **Re**, **Nu**) quantities. The calculated quantities have been calculated from the measured quantities and the fluid properties taken from REFPROP version 9.1. The uncertainties in the calculated quantities are due to the uncertainties in the measured quantities.

Non Boussinesq	Boussinesq
Ra$= 6.9 \cdot 10^8$	**Ra**$= 6.7 \cdot 10^8$
Pr$= 4.33$	**Pr**$= 7.24$
Water, $T_m = 40$°C	Methanol, $T_m = 20$°C
$\Delta T = 40$°C	$\Delta T = 9.6$°C
$\frac{\alpha_{bottom}-\alpha_{top}}{\alpha_{top}} = 153\%$	$\frac{\alpha_{bottom}-\alpha_{top}}{\alpha_{top}} = 1.5\%$
$\frac{\nu_{bottom}-\nu_{top}}{\nu_{top}} = -52\%$	$\frac{\nu_{bottom}-\nu_{top}}{\nu_{top}} = -13\%$

Quantity	Water	Methanol
H	0.7 %	
∇T	0.5 %	2.1 %
U	2 %	
U_{RMS}	4 %	
Ra	4.2 %	4.9 %
Pr	0.8 %	0.9 %
Re	3.3 %	3.4%
Nu	1.3 %	3.6 %

3.1 Contour Plots

Here some characteristics of the velocity field are described in a qualitative way with contour plots. A quantitative description, together with a comparison between the Boussinesq case and the NB case, is given in Section 3.2.

3.1.1 Time-averaged Velocities

The time average of the velocity field on a vertical cross section of the domain at half depth ($Z/H = 0.5$) is reported in Figure 4. The NB case is represented on the left, the Boussinesq case on the right. By comparing them it can be seen that the velocity fields show the same shape: a large big roll in the center, which characterizes the large scale circulation of the flow and two small counter-rotating rolls at the upper left corner and at the bottom right corner. This shape agrees with what has been previously observed by Xia et al. 2003 [7] at the same Rayleigh number, at Boussinesq conditions. Thermal plumes which erupt from the bottom boundary layer and impinge on the top one and vice versa are expressions of the driving force of the large scale circulation in this kind of flow. By comparing the two cases it is also possible to observe that the magnitude of the velocity field is lower for methanol than for water. This is mainly due to the fact that the two fluids have different properties. In Figure 5 the horizontal and vertical components of the mean velocity fields are represented both at Boussinesq and at NB conditions. It can be seen that the contour plots of the two cases have approximately the

same shape, but differ in magnitude. For each experiment 10,800 frames have been acquired during one hour long measurements. The statical uncertainty of the average value has been conservatively estimated as 2% of its measured value.

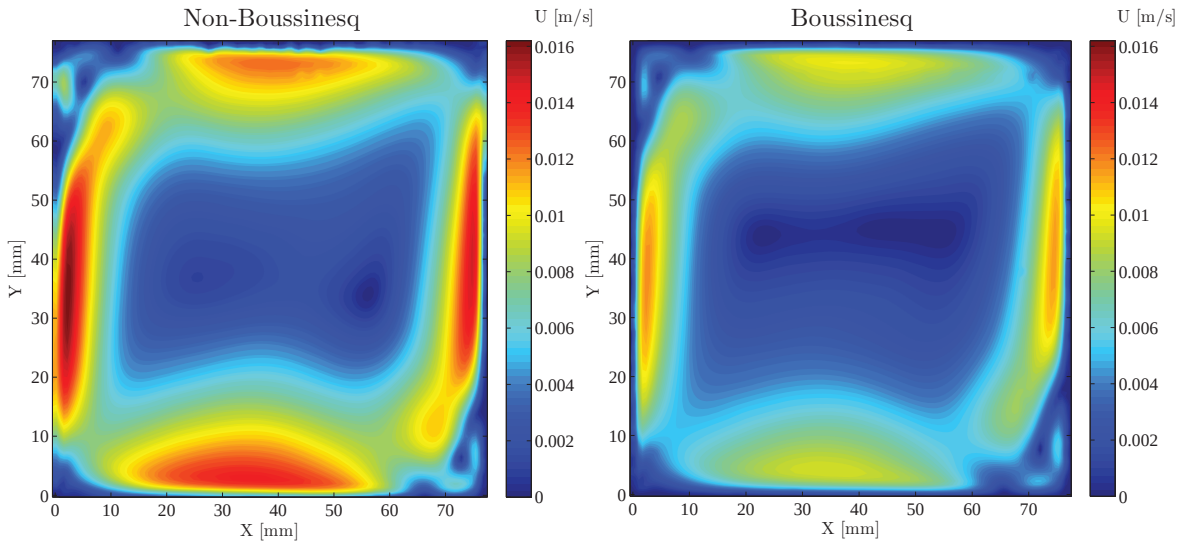

Figure 4: Time average velocities contour plots on a vertical cross section of the cell at half depth of the domain. Left) NB, $\mathbf{Ra} = 6.9 \cdot 10^8$, $\mathbf{Pr} = 4.33$, Right) Boussinesq, $\mathbf{Ra} = 6.7 \cdot 10^8$, $\mathbf{Pr} = 7.24$.

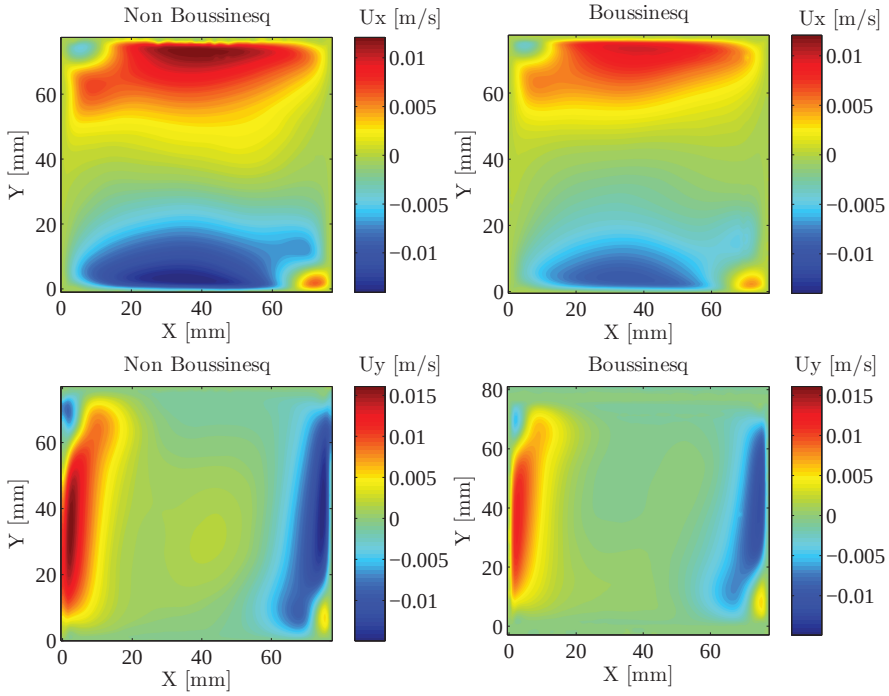

Figure 5: Time average velocity components contour plots on a vertical cross section of the cell at half depth of the domain. Left column) NB, $\mathbf{Ra} = 6.9 \cdot 10^8$, $\mathbf{Pr} = 4.33$. Right column) Boussinesq, $\mathbf{Ra} = 6.7 \cdot 10^8$, $\mathbf{Pr} = 7.24$. Top) Horizontal component, Bottom) Vertical component.

3.1.2 Turbulent kinetic energy

The turbulent kinetic energy components at $Z/H = 0.5$, are shown in Figure 6. At the top the RMS of the horizontal component of the velocity U_X is plotted both for the NB case (left) and Boussinesq case (right). The two contour plots show a similar shape, but a difference in magnitude. For both the Boussinesq and NB case the regions with the highest values of the RMSs are close to the corners. The peaks of the RMSs can be related to the shape of the large scale circulation reported in the plots on the first row of 5 and to its gradients. In particular it is possible to observe two peaks of the RMSs in correspondence to the two counter rotating rolls at the left top corner and at the right bottom one. The two small counter rotating rolls lead to fluctuations of the mean flow, which are visible in the RMSs plots.

Also for the vertical component of the velocity, U_Y, one can observe two peaks in the RMSs values at the top left corner and at the bottom right corner, corresponding to the two counter rotating rolls. The fluctuations of the velocity indeed are higher in the two regions immediately before the impingement of the big roll onto the two horizontal plates. This impingement generates the two counter rotating rolls.
The statistical uncertainty on the RMSs values has been conservatively estimated as 4% of their measured value.

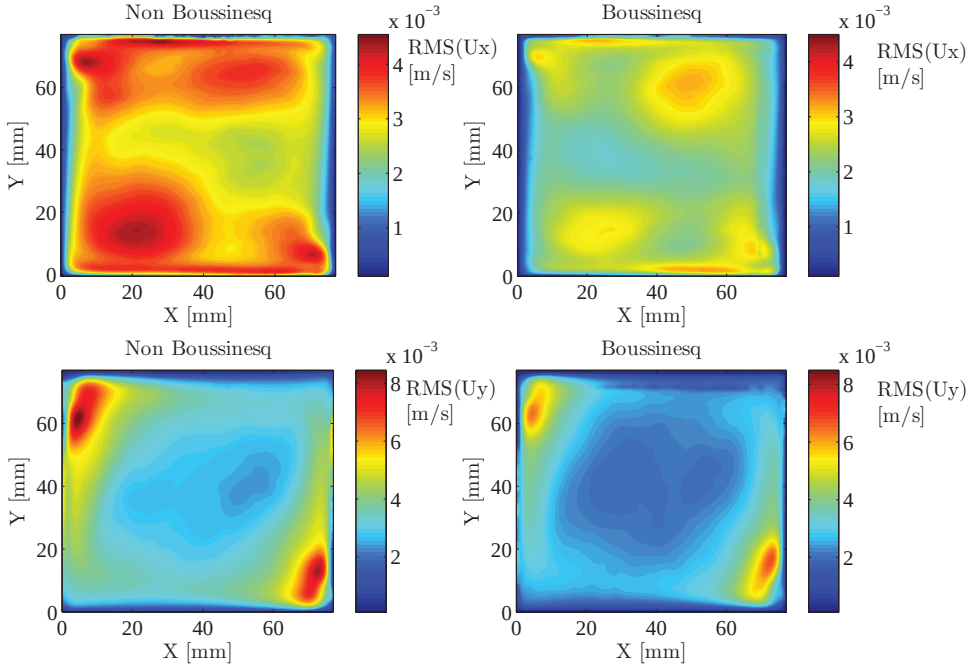

Figure 6: RMSs of the velocity components plotted on a vertical cross section of the cell at half depth of the domain. Left column) NB, $\mathbf{Ra} = 6.9 \cdot 10^8$, $\mathbf{Pr} = 4.33$. Right column) Boussinesq, $\mathbf{Ra} = 6.7 \cdot 10^8$, $\mathbf{Pr} = 7.24$. Top) Horizontal component, Bottom) Vertical component.

3.2 Profiles at mid-height and mid-width.

3.2.1 Qualitative description

In this section the values of the components of the velocity and of their RMSs are compared at $X/H = 0.5$ and at $Y/H = 0.5$ for the vertical and the horizontal components of the velocity and

of their RMSs, respectively. From Figure 7 it can be seen that, in accordance with the contour plots, the velocities and RMSs for both water and methanol have a similar shape. Moreover, the slope of U_X with respect to the Y coordinate shows three distinct slopes in the center region, as previously found by Xia *et al.* 2003, [7] at similar Rayleigh number at Boussinesq conditions. Moreover, the lower and the upper slopes have a similar value (for example around 2.6 s^{-1} for methanol), while the value of slope at the center (for example around 9 s^{-1} for methanol) differs significantly from the other two.

Looking at the shape of the RMSs values of U_X at $X/H = 0.5$, four peaks can be observed, corresponding to the regions of high shear, i.e. where the gradient of the horizontal component of the velocity U_X with respect to the Y coordinate is maximal. Apparently, the gradients dU_X/dY in the central region are large enough to cause a peak in the local RMS of U_X.
Looking at the shape of the RMSs values of U_Y at $Y/H = 0.5$, one can observe two peaks near the walls, due to the high values of the large scale circulation close to the wall.

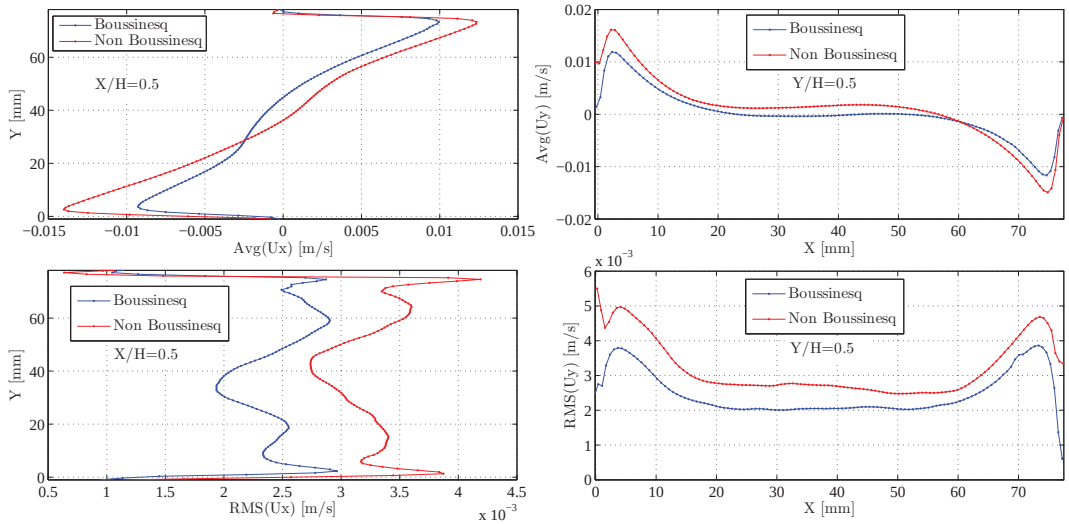

Figure 7: One line comparison between time average and RMSs velocity components. NB case: $\mathbf{Ra} = 6.9 \cdot 10^8$, $\mathbf{Pr} = 4.33$. Boussinesq case: $\mathbf{Ra} = 6.7 \cdot 10^8$, $\mathbf{Pr} = 7.24$. Left column) Comparison between the time average velocities (top) and their RMSs (bottom) at $X/H = 0.5$. Right column) Comparison between the time average velocities (top) and their RMSs (bottom) at $Y/H = 0.5$. Note: the first two points of the RMS(Uy) for the non-Bousinesq case are probably not reliable, because of wall reflections.

3.2.2 Quantitative comparison between Boussinesq and NB conditions

The Grossmann-Lohse (GS) theory, summarized in Ahlers *et al.* [8] allows the prediction of the Reynolds and the Nusselt, numbers as functions of the Rayleigh and Prandtl numbers.
The GS theory starts with two exact relations for the kinetic and thermal dissipation rates. Beside the use of the Boussinesq equations, further assumptions are about the presence of only one large scale circulation velocity, a single thickness of the kinetic boundary layers, homogeneous and isotropic turbulence in the bulk, application of the Prandtl-Blasius laminar boundary layer theory to the kinetic and thermal boundary layers and Peclet number close to zero (contribution of the molecular transport).

$$(\mathbf{Nu} - 1) \cdot \mathbf{Ra} \cdot \mathbf{Pr}^{-2} = c_1 \cdot \frac{\mathbf{Re}^2}{g\left(\sqrt{\mathbf{Re_c}/\mathbf{Re}}\right)} + c_2 \cdot \mathbf{Re}^3 \tag{5}$$

$$\mathbf{Nu}-1=c_3\cdot\mathbf{Re}^{1/2}\cdot\mathbf{Pr}^{1/2}\cdot\left\{f\left[\frac{2\cdot a\cdot\mathbf{Nu}}{\sqrt{\mathbf{Re}_c}}g\left(\sqrt{\frac{\mathbf{Re}_c}{\mathbf{Re}}}\right)\right]\right\}^{1/2}+c_4\cdot\mathbf{Pr}\cdot\mathbf{Re}\cdot f\left[\frac{2\cdot a\cdot\mathbf{Nu}}{\sqrt{\mathbf{Re}_c}}g\left(\sqrt{\frac{\mathbf{Re}_c}{\mathbf{Re}}}\right)\right] \tag{6}$$

These coupled equations are based on several assumptions, such as Boussinesq conditions and have been validated under specific conditions: $3\cdot10^7\leqslant Ra\leqslant3\cdot10^9$and $4\leqslant Pr\leqslant34$, for an aspect ratio one cylindrical cell. The aspect ratio of a cell is defined as the ratio between the horizontal and the vertical dimension of the domain.
For the current study, the following constants and formulas need to be applied:

$$\mathbf{Re}_c=1.0,\ c_1=8.7,\ c_2=1.45,\ c_3=0.46,\ c_4=0.013,\ a=0.482 \tag{7}$$

$$f(x_\theta)=(1+x_\theta^4)^{-1/4},\ x_\theta=2\cdot a\cdot\frac{\mathbf{Nu}}{\sqrt{\mathbf{Re}}} \tag{8}$$

$$g(x_L)=x_L\cdot(1+x_L^4)^{-1/4},\ x_L=\sqrt{\frac{\mathbf{Re}_c}{\mathbf{Re}}} \tag{9}$$

The six parameters c_1, c_2, c_3, c_4, a and Re_C are dimensionless prefactors obtained, as explained in [10], by fitting experimental data in the **Ra** and **Pr** range above indicated. The function $f(x_\theta)$ is a cross-over function proposed in [10] in order to describe the transition from Prandtl number smaller to bigger than one. The variable x_θ expresses the ratio of the kinematic and thermal boundary layer thickness. The function $g(x_L)$ is a cross-over function proposed in [10] to model the very large **Pr** regime. In this regime the thickness of the kinetic boundary layer does not increase anymore with decreasing **Re**, but it saturates towards a constant value with order of magnitude of the height of the convection cell. $\mathbf{Re}_c$ is a value of the **Re** number used in [10] when at very large **Pr** numbers the flow eventually becomes laminar.
The constant a in equations (6) and (8) is a non-dimensional prefactor used to define the absolute value of the kinetic boundary layer thickness, assuming a laminar boundary layer with a Prandtl-Blasius profile, as explained in Grossmann and Lohse (2002)[11].
Both **Ra** and **Pr** are known (from the experiments), hence by solving equations (5) and (6) the **Nu** and **Re** numbers can be found. The **Nu** number can be used to determine the theoretical heat flux required to keep the bottom and top walls on the required temperatures. By comparing this theoretical heat flux to the experimental one, the heat losses to the environment, by radiation and convection and also the transferred heat by conduction through the glass lateral walls of the cell can be estimated.
The Nusselt number can be measured supposing that all the electrical power given to the heating strip of the bottom plate of the cell is transferred trough the fluid to the top plate. It can be calculated using equation (4) with $Q=P/A$, where P is the electrical power given to the electric strip of the bottom plate and $A=H^2$ is the surface of the plate.
The difference between the theoretical and the measured **Nu** numbers is quite small for both the Boussinesq and the NB case, assuring that the heat losses are small. In particular the theoretical **Nu** number for the NB case is around 59, while the measured one is 58. For the Boussinesq case the theoretical **Nu** number is around 58, while the experimental one is around 59. The **Nu** numbers of both the Boussinesq and the NB case are well predicted by the GS theory and the heat losses of the experiments can be considered negligible.

The **Re** number can be used to make the velocities non-dimensional with the integral velocity scale. The entire flow problem can therefore be made non-dimensional and, most importantly, *can be made independent of the fluid used*, facilitating the comparison between the Boussinesq case (i.e. methanol) and the NB case (i.e. water).

The non-dimensional values of the average velocity ($U_i \cdot H/\nu_m$) and of their RMSs ($\sqrt{\overline{U_i' U_i'}} \cdot H/\nu_m$) at both NB and Boussinesq conditions can be found in Figure 8, where the Boussinesq experiment has been multiplied for ($\mathbf{Re}_W/\mathbf{Re}_M$), which is the ratio of the **Re** number obtained from the formulas (5) and (6) for the water experiment and the **Re** obtained for the methanol case. This ratio has been found to be 1.43. It can be seen that the above methodology results in almost collapsing plots, indicating the validity of the model proposed by Grossmann and Lohse [8] also for the NB case. The fact that the scaled curves collapse agrees with what has been numerically confirmed by Sugiyama *et al.* 2009, [6], but has never before been proven experimentally.

Although there is a rather close agreement between both the Boussinesq and NB case, some differences are found. At NB conditions, the magnitude of the horizontal velocity component $U_X \cdot H/\nu_m$ close to the bottom wall is higher than that of the Boussinesq case. Moreover, the peak close to the bottom wall is higher than the peak close to the top wall, whereas the peaks for the Boussinesq case are the same. These findings are most probably related to the fact that the kinematic viscosity close to the bottom wall is significantly lower than its value close to the top wall at NB conditions, resulting in a higher velocity gradient. To a lesser extent, such behavior is visible for the profiles of $U_Y \cdot H/\nu_m$ as well. The peak at low X-values is approximately 7% larger for the NB case, being outside the uncertainty of 2%. Besides the near-wall peaks in the velocity profiles, there is a small differences in the center region which needs further investigation.

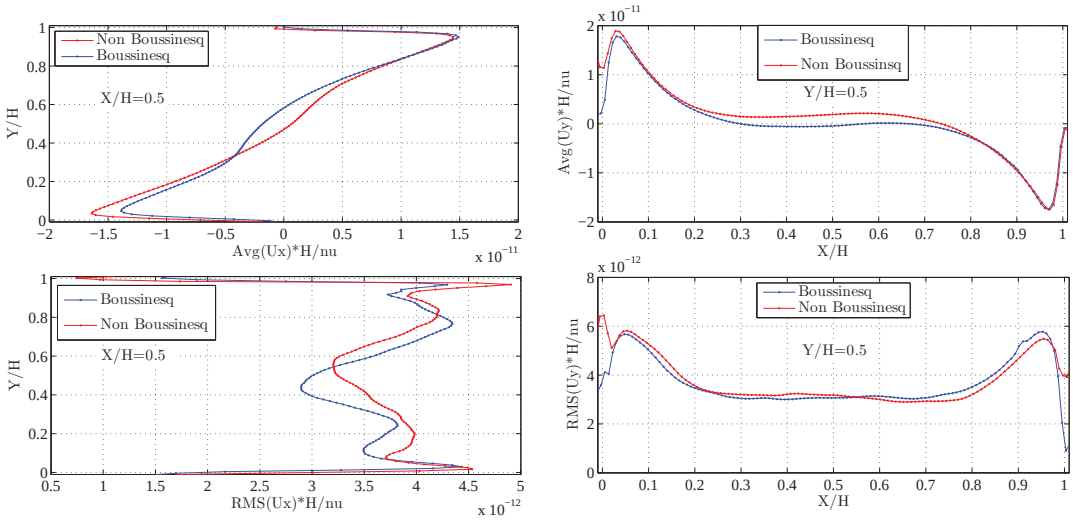

Figure 8: One line comparison between scaled and non dimensional time average and RMSs velocity components. Non Boussinesq case: $\mathbf{Ra} = 6.9 \cdot 10^8$, $\mathbf{Pr} = 4.33$. Boussinesq case (velocities and RMS scaled): $\mathbf{Ra} = 6.7 \cdot 10^8$, $\mathbf{Pr} = 7.24$. Left column) Comparison between the time average velocities (top) and their RMSs (bottom) at $X/H = 0.5$. Right column) Comparison between the time average velocities (top) and their RMSs (bottom) at $Y/H = 0.5$. The values of the velocities and their RMSs have been non-dimensionalized using the value of the kinematic viscosity at the medium temperature between the temperatures of top and bottom plates. Note: the first two points of the RMS(Uy) for the non-Bousinesq case are probably not reliable, because of wall reflections.

4 CONCLUSIONS

In the present paper the influence of variable fluid properties on a natural convection system have been investigated experimentally.

Particle Image Velocimetry measurements of a Rayleigh-Bénard flow both at NB and at Boussinesq conditions have been done with the aim of comparing the flow structure at NB conditions with respect to Boussinesq conditions.
Good agreement has been found between the experiments and the GL theory, which was able to predict also the Reynolds number at the NB condition studied experimentally. After scaling, the average velocities and RMSs values of the NB and Boussinesq cases collapse quite well.
Besides a global agreement between the Boussinesq and NB case, there are also same small differences, which can be related to the effect of temperature varying properties. In particular the horizontal component of the average velocity shows a slight asymmetry which may be due to the higher kinematic viscosity close to the bottom wall with respect to viscosities close to the top wall, at NB conditions. To a lesser extent a slight asymmetry has been observed also for the vertical component of the average velocity in the NB case.

The findings of the present study are the base for a future experimental study at supercritical pressure, where not only the kinematic viscosity and the volumetric thermal expansion coefficient significantly change with temperature, but also the other properties and in a more profound manner than at atmospheric pressure. A Rayleigh-Bénard set-up has been designed with the purpose of working at supercritical pressure with Freon, allowing us also the possibility to perform optical measurements in it, like it has been done in a simpler way at atmospheric pressure.
The present study can therefore be used as experimental base on the effects of variable properties on turbulent natural convection, for the understanding of the different heat transfer regimes in supercritical fluids and the development of HPLWRs.

NOMENCLATURE

Greek symbol	Description	Dimension
α	volumetric thermal expansion coefficient	$[K^{-1}]$
λ	thermal conductivity	$\left[\frac{W}{m \cdot K}\right]$
κ	thermal diffusivity	$\left[\frac{m^2}{s}\right]$
ν	kinematic viscosity	$\left[\frac{m^2}{s}\right]$
∇T	temperature difference between the top and the bottom plate of the cell	[K]
Γ	aspect ratio of the cell (ratio between the horizontal and the vertical dimensions of the cell)	
Latin symbol	Description	Dimension
a	non-dimensional prefactor of the GL theory	
c_1, c_2, c_3, c_4	non-dimensional prefactor of the GL theory	
g	gravitational acceleration	$\left[\frac{m}{s^2}\right]$
$\mathbf{Re}_c$	value of the Re number used in the GL theory at very large Pr numbes	
A	surface of a face of the cubical cell	$\left[m^2\right]$
H	dimension of the cubical cell	[m]
P	electrical power given by the heating strip at the bottom of the cell	$[W]$
Q	heat flux trough the cell	$\left[\frac{W}{m^2}\right]$
U	velocity of the large scale circulation	[m/s]
X	horizontal axis	[m]
Y	vertical axis	[m]
Z	horizontal axis nomal to the plane XY	[m]

Non dimensional number	
Nu	Nusselt number
Pr	Prandtl number
Ra	Rayleigh number
Re	Reynolds number
Subscript	
bottom	bottom plate of the cell
i	generic coordinate, either X or Y
m	average between the value of a property at the top of the cell and the value of the same property at the bottom of the cell
top	top plate of the cell
M	methanol
W	water
Abbreviation	Description
Avg	Average
BWR	Boiling Water Reactor
DNS	Direct Numerical Simulations
GL	Grossmann-Lohse
HPLWR	High Performance Light Water Reactor
NB	Non Boussinesq
NPP	Nuclear Power Plant
NTC	Negative Temperature Coefficient
PIV	Particle Image Velocimetry
RB	Rayleigh-Bénard
RMS	Root Mean Square
SCWR	Super Critical Water Reactor
2D	2 Dimensional

ACKNOWLEDGMENT

This research is supported by the Dutch Technology Foundation STW, which is part of the Netherlands Organization for Scientific Research (NWO), and which is partly funded by the Ministry of Economic Affairs

References

[1] I. L. Pioro, H. F. Khartabil, R. B. Duffey, "Heat transfer to supercritical fluids flowing in channels-empirical correlations (survey)", *Nuclear Engineering and Design*, **Vol. 230**, pp. 69–91, (2004)

[2] V.A. Kurganov, A.G. Kaptil'ny, "Velocity and enthalpy fields and eddy diffusivities in a heated supercritical fluid flow", *Exp. Therm. Fluid Sci.,* **Vol. 5**, pp. 465-78, (1992)

[3] J. Y. Yoo, "The Turbulent Flows of Supercritical Fluids with Heat Transfer", *Annual Review of Fluid Mechanics*, **Vol. 45**, pp. 495-525, (2013)

[4] J. Fewster, J.D. Jackson, "Experiments on Supercritical Pressure Convective Heat Transfer Having Relevance to SPWR", *Proceedings of the 2004 international congress on advances in nuclear power plants*, Pittsburgh, PA (United States), 13-17 Jun 2004, **Vol. 40**, pp. 537-551, (2004)

[5] G. Ahlers, E. Brown, F. Fontanelle Araujo, D. Funfshilling, S. Grossmann and D. Lohse, "Non-Oberbeck-Boussinesq effects in strongly turbulent Rayleigh-Bénard convection", *Journal of Fluid Mechanics*, **Vol. 569**, pp. 409-445, (2006)

[6] K. Sugiyama, E. Calzavarini, S. Grossmann and D. Lohse, " Flow organization in two-dimensional non-Oberbeck-Boussinesq Rayleigh-Bénard convection in water", *Journal of Fluid Mechanics*, **Vol.** 637, pp. 105-135, (2009)

[7] K.-Q. Xia, C. Sun, and S.-Q. Zhou, "Particle image velocimetry measurement of the velocity field in turbulent thermal convection", *Phys. Rev. E*, **Vol. 68**(6), pp.066303 1-18, (2003)

[8] G. Ahlers, S. Grossmann, and D. Lohse, "Heat transfer and large scale dynamics in turbulent Rayleigh-Bénard convection", *Rev. Mod. Phys.*, **Vol. 81**(2), pp. 503-537, (2009)

[9] M. Steunebrink, M.J. Tummers, H.J.J. Honker, "Effect of surface roughness on flow and heat transfer in Rayleigh-Bénard convection", Chapter 3, MSc Thesis, Delft University of Technology, Delft, The Nethederlands, (2013)

[10] S. Grossmann and D. Lohse, "Thermal convection for large Prandtl Numbers", *Phys. Rev. Lett.*, **Vol. 86**(15), pp.3316 -3319, (2001)

[11] S. Grossmann and D. Lohse, "Prandtl and Rayleigh number dependence of the Reynolds number in turbulent thermal convection", *Phys. Rev. E*, **Vol. 66**, pp.016305 1-6, (2002)